Proof-of-Principle Experiment on the Dynamic Shell for Inertial Confinement Fusion

I. V. Igumenshchev, W. Theobald, C. Stoeckl, R. C. Shah, D. Bishel, V. N. Goncharov,*
M. J. Bonino, E. M. Campbell, L. Ceurvorst, D. A. Chin, T. J. B. Collins, S. Fess, D. R. Harding,
S. Sampat, N. R. Shaffer, A. Shvydky, W. T. Trickey, and L. J. Waxer
*Laboratory for Laser Energetics, 250 East River Road, Rochester, New York 14623-1212, USA**

A. Colaïtis and R. Liotard
Centre Lasers Intenses et Applications, UMR 5107,
351 Cours de la libération, 33400 Talence, France

P. Adrian
Plasma Science and Fusion Center, MIT, Boston, MA, USA

S. Atzeni, F. Barbato, and L. Savino
Dipartimento SBAI, Universitá degli Studi di Roma "La Sapienza", Roma, Italy

N. Alfonso, A. Haid, and Mi Do
General Atomic
(Dated: February 1, 2023)

The dynamic-shell (DS) implosion concept in inertial confinement fusion utilizes a ball of liquid DT, which is first compressed by convergent shocks, then expands after bouncing these shocks from the center, decelerates and forms a shell with the help of following subsequent converged shocks, and finally, the shell is imploded igniting the DT fuel as in conventional central hot-spot ignition. Proof-of-principle experiments on the OMEGA laser have demonstrated, for the first time, the feasibility of directly driven DS formation in a spherically expanding cloud of plasma. A shell is formed by convergent shocks launched at the edge of the cloud, with the cloud itself formed as a result of compression and relaxation of surrogate plastic-foam ball targets. Three x-ray diagnostics, 1-D self-emission spatially resolver streaked imaging and 2-D self-emission framed imaging and backlighting radiography, have shown good agreements with the predicted evolution of the DS and its stability to low-mode perturbations introduced by laser irradiation and target asymmetries.

The dynamic-shell (DS) concept in inertial confinement fusion (ICF) utilizes the conventional hot-spot ignition scheme [1] and uses a cryogenic liquid ball targets of deutrium–tritium (DT) as a fuel that is dynamically shaped into a shell by the application of a carefully designed train of laser pulses [2]. These shell shaping and ignition are accomplished in four evolution stages. In the first stage, a liquid DT ball target is compressed by a few-Mbar convergent shock wave, which is launched by intense laser beams symmetrically irradiating the target. The second stage starts when this shock reaches the target center, reflects, and is transformed into a blast wave, causing the shock-compressed mass to expand. The third stage begins with launching several convergent shocks at the outer edge of the expanding mass. These shocks decelerate and reverse the expansion, resulting in a dynamic formation of a dense shell. In the final fourth stage, this shell is imploded using a powerful laser pulse similar to that in the conventional direct-drive hot-spot ignition scheme.

High-gain ($G \sim 100$, where the gain G is the ratio of fusion energy to laser energy) DS ignition designs require low-adiabat ($\alpha \lesssim 2$, where the adiabat α is the ratio of the plasma pressure to the Fermi-degenerated pressure) imploding shells. Such shells can be formed either with an appropriately time-shaped continuous pulse or with a sequence of short picket pulses (∼200- to 300-ps duration). Pickets have the advantages discussed in Ref. [2]. Example 1-D simulations of a high-gain DS design using the multidimensional radiation-hydrodynamic code *ASTER* [3] are illustrated in Fig. 1, which shows a "shock diagram" (a plot of log-density evolution) in color scale. This design uses a 1.3-MJ laser pulse, which is shown by the blue line, and a 3280-μm-diam cryogenic liquid DT ball target with a wetted-foam addition layer that is shown in Fig. 2(a). The pulse is about 210-ns long and consists of 12 pickets and a final ramp compression pulse. Here, the first three pickets launch three shocks that initially compress the target (the first stage). Trajectories of these shocks are seen in Fig. 1 as the three contrast-density lines on the left in the color-scaled image. These shocks merge and bounce from the center at $t = 63$ ns, resulting in a blast wave and an expansion of the target mass (the second stage). The next eight pickets starting at $t = 50$ ns launch a sequence of eight shocks that decelerate the expanding plasma cloud and form a dense shell (the third stage). The last picket at $t = 188$ ns and the following ramp-compression pulse drive low-adiabat

* Also at Department of Mechanical Engineering, University of Rochester, Rochester, New York 14623, USA

implosion, resulting in ignition with $G = 100$ (the fourth stage).

The DS concept has a number of advantages over other ICF concepts. These advantages include, among others, the relative simplicity of fabrication of a cryogenic liquid ball target (since no layering of a solid DT shells is required) with a potentially smoother target surface with less defects seeding perturbations than a solid cryogenic DT shell. Such a target is approapriate for mass production required for commercial power plants. The large parameter space of DS designs introduces the flexibility of varying the convergence ratio of implosion shells [2] and changing their stability properties. The DS concept is compatible with the central hot-spot and shock-ignition approaches.

On the downside, the DS concept requires complicated laser pulses that are not available on current laser systems. These pulses result in complicated target dynamics affecting the evolution of various perturbations, caused, e.g., by target imperfections, target offset, laser beam pointing, and laser imprint. The formation of the DS and its sensitivity to such perturbations should be addressed experimentally and by systematic simulation studies.

This Letter describes results of a proof-of-principle experiment on the OMEGA laser [4] that demonstrates, for the first time, the feasibility of directly driven DS formation using a scaled-down experimental setup to acommodate the limitations in the available laser energy ($\lesssim$20 kJ) and the pulse duration ($\leq$4 ns). The experiments use room-temperature surrogate spherical targets consisting of a CH foam with a mass density of 0.130 g/cm^3 and an outer diameter of about 600 μm [see Fig. 2(b)]. The use of foam lets one avoid the complexity of handling cryogenic targets and introduces the convenience of varying the foam density.

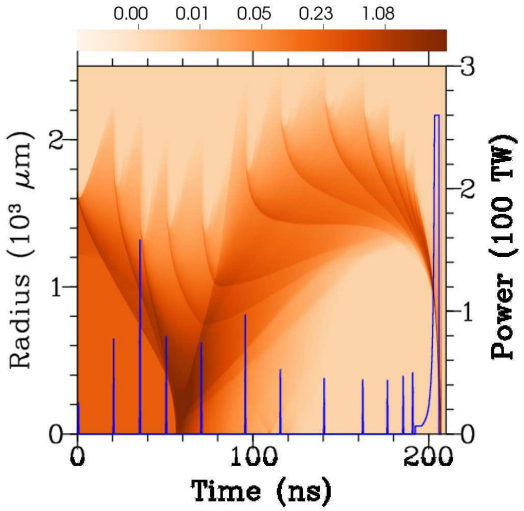

FIG. 1. Laser power history (blue line) for an ingition DS design using the target shown in Fig. 2(a). The graded color image shows the log-density evolution (a "shock diagram") from 1-D simulations. The upper bar indicates the log-density scale in g/cm^3. The density interfaces indicate spherical convergent or divergent shock waves.

The target is attached to a solid plastic (CH) mount stalk of 50 μm in diameter. The target and stalk were printed simultaneously using the two-photon polymerization (2PP) technique [5]. The foam is built using the body-centered-cubic lattice structure. Each lattice node is connected to others by eight fibers of about 8 μm in length, each having an approximately elliptical cross section with dimensions of about 2.3×0.7 μm. These fibers are arranged in space such that their projected thickness takes the minimum (0.7 μm) in the direction of stalk, and the maximum (2.3 μm) in the perpendicular directions. Therefore, the target foam has larger pore sizes along the stalk. This foam asymmetry is likely the reason of an observed mod-2 implosion asymmetry discussed later.

As an example, the laser pulse of shot 105251 is shown in Fig. 3(a) by the black line. It consists of two square pulses of about 0.5- and 2-ns duration, respectively, with a 1-ns gap between them. The second pulse ends with a power spike. The total pulse energy was 11.2 kJ and the duration was about 4 ns. Sixty laser beams were focused on target using SG5-650 distributed phase plates [6], each of which produces a spot with the super-Gaussian profile of the order of 4.2 and $R_b = 337$ μm, where R_b is the radius incirculating 95% of the beam energy. The beams were smoothed by polarization smoothing [7] and smoothing by spectral dispersion [8] at 0.3-THz bandwidth and three color cycles [9].

Foam targets in the OMEGA experiment undergo the same evolution stages (compression, expansion, shell formation, and implosion) as cryogenic targets in the DS ignition design. Figure 3(a) illustrates these stages showing the simulated shock diagram for shot 105251. The first square pulse launches a shock that initially compresses the target. This shock bounces from the center at $t = 1.4$ ns, forming a blast wave and resulting in expansion of the compressed target mass. The second square pulse, which starts at $t = 1.8$ ns, decelerates the expanding plasma and forms a dense shell. The outer shell radius, which is defined as the radius of the ablation front and seen as a density interface in Fig. 3(a), is initially reduced to about 180 μm at 2.15 ns, then increased reaching about

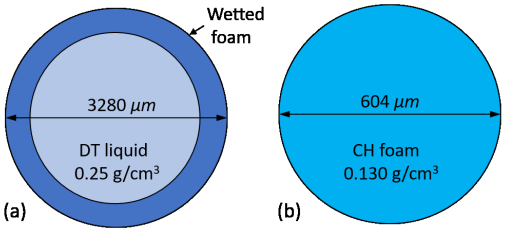

FIG. 2. (a) Spherical liquid-DT target for the ignition DS design. (b) Surrogate foam ball target used in OMEGA shot 105251.

200 μm at 2.8 ns, and then decreased again approaching the minimum of about 120 μm at 4.0 ns. A thin, dense shell of outer radius of about 150 μm is formed at $t \approx 3.8$ ns. The power spike at the end of the pulse helps to additionally compress the shell, increasing the contrast in density. The use of square pulses instead of picket pulses in the ignition design (see the blue curve Fig. 1) results in developing a relatively high-adiabat shell, which is less succeptible to the high Legendre mode ($\ell \gtrsim 30$) perturbation growth.

The experiments employed three x-ray diagnostics to evidence the DS formation. These include a streaked self-emission 1-D imaging [10], framed self-emission shadowgraphy [11], and backlighting radiography [12]. Figure 3(b) shows the streaked data obtained in shot 105251. The streak camera detector collects x rays at around 1 keV. These data can be compared with a synthetic streak image in Fig. 3(c) from post-processing 1-D *ASTER* simulations, which include cross-beam energy transfer (CBET) [13] and assume Spitzer–Härm heat conduction [14] with the electron free-streaming flux limitation. Nearly identical streak images were obtained using *DUED* hydrodynamic simulations [15] (using the sharp-cutoff flux-limiter of 0.07 and omitting CBET, but reducing laser power by about 15% to account for CBET losses) and related postprocessors. Figures 3(b) and 3(c) show vertically extended bright spots between $t = 0$ and 1 ns, corresponding to emission from the target surface caused by the leading square laser pulse. The discrepancy in the shape of the measured and simulated spots can be attributed to high-z debris unintentionally collected on the outer surface of targets during their handling. Several tens of such debris of about several micron in size were observed on the surface of each target on pre-shot images. They are likely the cause of nonuniform emission and were not accounted in simulations.

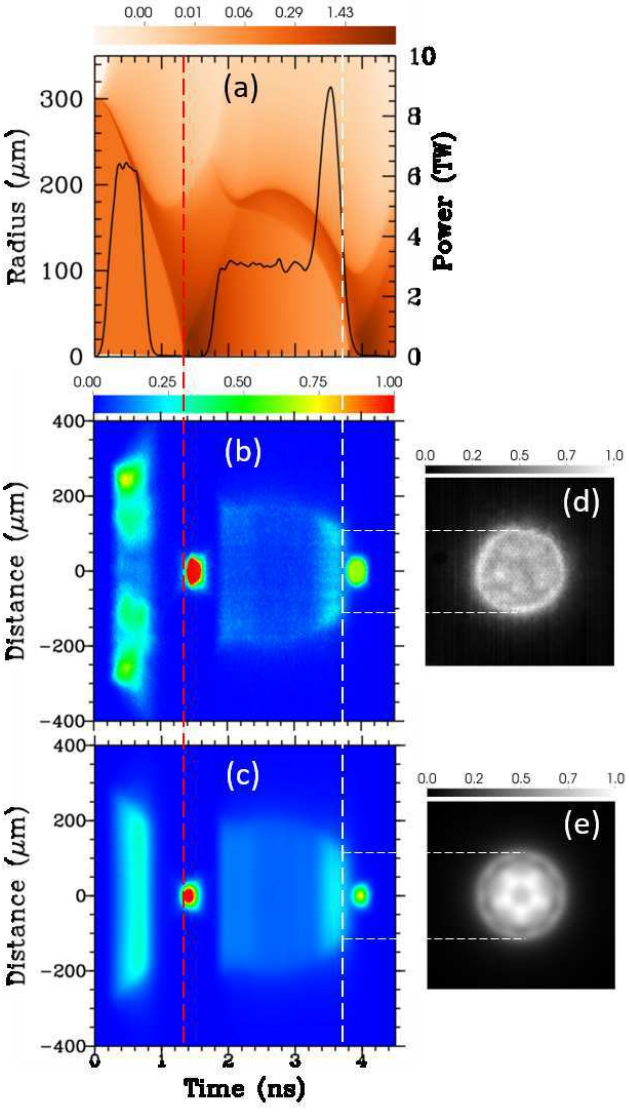

FIG. 3. (a) Laser power history (black line) and simulated shock diagram (graded color image) for OMEGA shot 105251 using the target shown Fig. 2(b). For the same shot: (b) and (c) streaked measured and simulated self-emission radiographs, respectively; (d) and (e) framing camera measured and simulated shadowgraphs, respectively.

The bright red spot at $t \approx 1.5$ ns in Fig. 3(b) is the signature of emission from the first shock bounce [see Fig. 3(a); the vertical red dashed line indicates time of the bounce]. The onset of this emission is accurately reproduced in simulations [see Fig. 3(c)] within the uncertainty of the absolute timing of the diagnostic (∼10 ps). These results are in good agreements with *ASTER* simulations using the 3-D ray-trace code *IFRIIT* [16] and a recently developed solid-to-plasma transition model [17] for foams, including the effect of shinethrough, which did not show significant influence on shock timing and areal-density evolution for the considered high-adiabat design.

The next bright region in Fig. 3(b) starts with the beginning of the second square laser pulse at $t = 1.8$ ns and corresponds to emission from the ablation surface of the decelerating expanding plasma cloud. The top and bottom rims of this region represent the ablation surface trajectory, which is observed in the shock diagram in Fig. 3(a) as the outer contrast-density line. The synthetic streak in Fig. 3(c) reproduces the measured trajectory with good agreement. Note that even the structure of the bright region in Fig. 3(b), including the images of vertical strips, is well reproduced in simulations [compare with Fig. 3(c)].

The second bright spot at $t \approx 4.0$ ns [green-yellow spot in Figs. 3(b)] is the signature of the collapse of the dense shell that is seen in Fig. 3(a). Note that simulations predict the onset of this spot by about 50 ps later [see Fig. 3(c)].

Framing-camera measurements evidence the DS formation during the implosion stage. Figure 3(d) shows a self-emission x-ray image of DS target in shot 105251 at $t = 3.75 \pm 0.5$ ns. The vertical white dashed line in Figs. 3(a)–3(c) indicates $t = 3.75$ ns for convenience.

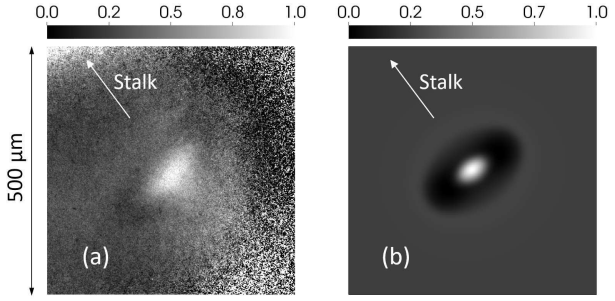

FIG. 4. (a) Measured and (b) simulated backlighting radiographs at the moment of stagnation of the dense shell for OMEGA shot 105249. The dark ellipse near the center is a shadow of the shell. The center bright spot corresponds to emission of hot-spot plasma resulting from the collapse of the shell.

The outer bright circular rim in the image in Fig. 3(d) is caused by the emission from a thin spherical layer of plasma outflowing form the ablation surface. The less-bright region inside the rim is developed because of shadowing by the dense shell the emission coming from the ablation surface on the opposite side of the target. Five almost symmetrically located bright spots inside the bright rim correspond to radiation diffusing out from the hot plasma interior of the dense shell. Simulations suggest that these spots appear at dips on the shell, with the dips themselves developed from perturbations caused by the OMEGA discrete-beam illumination. The five-spot symmetry in Fig. 3(d) is explained by the symmetry of the OMEGA beam-port configuration when viewing through the center of one of pentagons formed by the ports.

Figure 3(e) shows a synthetic x-ray self-emission image at $t = 3.75$ ns from post-processing 3-D *ASTER* simulations of shot 105251. This shadowgraph reveals similar features that are observed in Fig. 3(d): the outer bright rim, less-bright shadow inside the rim, and five symmetric bright spots. The latter spots, however, were found only in simulations, in which the lateral heat flux was reduced ($\times 0.05$ in the shown case), and were not found in nominal simulations using the full flux. Lateral heat flux near the ablation surface serves to smooth out hydrodynamic perturbations including those from overlapping OMEGA beams. An overestimation of such smoothing in nominal simulations could indicate missing physics (e.g., self-generated magntic fields) that affect the heat transport.

Backlighting radiography [12] used an infrared (1053-nm) 20-ps, 1.5-kJ short-pulse beam from the OMEGA EP laser [18] that was focused with an intensity of 3×10^{16} W/cm^2 onto a Si foil target with a CH side shield [19] for producing the Si He$_\alpha$ line emission at 1.865 keV that transmits through the shell target. This target was imaged by a shaped Bragg crystal onto single-strip x-ray framing camera. Figure 4(a) shows a radiographic image in shot 105249 that was obtained by firing the backlighting beam at $t = 4.0 \pm 0.03$ ns, corresponding to the time of stagnation of the imploding shell. Imaging was started at $t = 3.8 \pm 0.2$ ns and used about 400-ps integration time, so that the center bright spot, which is caused by the shell collapse and observed in Fig. 3(b), is observed in this radiograph as well. The shadow of the stagnated shell and center bright spot in Fig. 4(a) demonstrates a large mode-2 asymmetry, meaning that the shell takes an oblate spheroid shape with the aspect ratio of about 2 where the spheroid minor axis is closely aligned with the stalk.

Three-dimensional *ASTER/IFRIIT* simulations suggest that the effects of stalks and target offsets (typically $\lesssim 5$ μm) and typical errors in mispointing ($\lesssim 10$ μm) and power balance ($\lesssim 5\%$) of OMEGA laser beams are insufficient to explain the observed shell asymmetry. These simulations also suggest that such an asymmetry can result from a significantly nonuniform compression of the foam target during the initial compression stage. As an example, Fig. 4(b) shows a synthetic radiograph of a shell from simulations of shot 105249 assuming a temporally applied (from $t = 0$ to 1 ns) mode–2 perturbation in beam power with $\sigma_{\rm rms} = 20\%$ and with a shape in which more power is symmetrically supplied to beams perpendicular to the stalk. The shadow in this radiograph reasonably well reproduces the asymmetry of the shadow in Fig. 4(a), including its alignment with the stalk. The perturbations in this example mimic the actual perturbations, which can be attributed to the effects of foam structural asymmetry as discussed earlier. In such a case, the foam target, which is more porous along the stalk direction, is faster compressed by shocks in the tangential directions. The seeming disagreement between the tangential compression and the oblate shape the shell in Figs. 4(a) and 4(b) is explained by a phase inversion of the mode-2 perturbation during the shock bounce at $t = 1.4$ ns.

In summary, the proof-of-principle experiment on the OMEGA laser has demonstrated for the first time the feasibility of DS formation in the scaled-down setup using foam-ball targets. Three x-ray diagnostics employing streaked self-emission imaging, framing self-emission shadowgraphy, and backlighting radiography evidence the DS formation and showed good agreement with synthetic x-ray radiographs obtained post-processing the results of 3-D radiation-hydrodynamic simulations using the code *ASTER* coupled with the laser ray-tracing code *IFRIIT*. The developed DS's show good stability to low-mode perturbations including mode-1 perturbations because of mount stalks and target offsets, mode-2 asymmetry possibly developed because of the asymmetric foam structure, and mode-10 perturbations from overlapping OMEGA beams. Good agreement in timing of measured and predicted x-ray flashes from shock bounce indicates the plausibility of modeling foam dynamics assuming corresponding volume-averaged continuous medium. Nominal radiation-hydrodynamic simulations were incapable reproducing the observed mid-mode ($\ell \sim 10$) perturbations at the ablation front. This could indicate missing

physics that affect thermal smoothing of such perturbations.

ACKNOWLEDGMENTS

This material is based upon work supported by the Department of Energy National Nuclear Security Administration under Award Number DE-NA0003856 and ARPA-E BETHE Grant No. DE-FOA-0002212. The experiment was conducted at the Omega Laser Facility at the University of Rochesters Laboratory for Laser Energetics with the beam time through the National Laser Users Facility (NLUF) program.

[1] S. Atzeni and J. Meyer-ter-Vehn, *The Physics of Inertial Fusion: Beam Plasma Interaction, Hydrodynamics, Hot Dense Matter*, 1st ed., International Series of Monographs on Physics, vol. 125 (Oxford University Press, Oxford, 2004), p. 43.

[2] V. N. Goncharov, I.V. Igumenshchev, D. R. Harding, S.F.B. Morse, S. X. Hu, P. B. Radha, D. H. Froula, S. P. Regan, T.C. Sangster, and E. M. Campbell, Novel hot-spot ignition designs for inertial confinement fusion with liquid-deuterium-tritium spheres, Phys. Rev. Lett. **125**, 065001 (2020).

[3] I. V. Igumenshchev, V. N. Goncharov, F. J. Marshall, J. P. Knauer, E. M. Campbell, C J. Forrest, D. H. Froula, V. Yu. Glebov, R. L. McCrory, S. P. Regan *et al.*, Three-dimensional modeling of direct-drive cryogenic implosions on OMEGA, Phys. Plasmas **23**, 052702 (2016).

[4] T. R. Boehly, D. L. Brown, R. S. Craxton, R. L. Keck, J. P. Knauer, J. H. Kelly, T. J. Kessler, S. A. Kumpan, S. J. Loucks, S. A. Letzring *et al.*, Initial performance results of the OMEGA Laser System, Opt. Commun. **133**, 495 (1997).

[5] S. Maruo, O. Nakamura, and S. Kawata, Three-dimensional microfabrication with two-photon-absorbed photopolymerization, Opt. Lett. **22**, 132 (1997).

[6] W. Theobald, D. Cao, R. C. Shah, C. A. Thomas, I. V. Igumenshchev, K. A. Bauer, R. Betti, M. J. Bonino, E. M. Campbell, A. R. Christopherson *et al.*, Enhanced laser-energy coupling with small-spot distributed phase plates (SG5-650) in OMEGA DT cryogenic target implosions, Phys. Plasmas **29**, 012705 (2022).

[7] J. E. Rothenberg, Polarization beam smoothing for inertial confinement fusion, J. Appl. Phys. **87**, 3654 (2000).

[8] S. Skupsky, R. W. Short, T. Kessler, R. S. Craxton, S. Letzring, and J. W. Soures, Improved laser-beam uniformity using the angular dispersion of frequency-modulated light, J. Appl. Phys. **66**, 3456 (1989).

[9] S. P. Regan, J. A. Marozas, R. S. Craxton, J. H. Kelly, W. R. Donaldson, P. A. Jaanimagi, D. Jacobs-Perkins, R. L. Keck, T. J. Kessler, D. D. Meyerhofer *et al.*, Performance of 1-THz-bandwidth, two-dimensional smoothing by spectral dispersion and polarization smoothing of high-power, solid-state laser beams, J. Opt. Soc. Am. B **22**, 998 (2005).

[10] S. Ressel, J. J. Ruby, G. W. Collins, and J. R. Rygg, Density reconstruction in convergent high-energy-density systems using x-ray radiography and Bayesian inference, Phys. Plasmas **29**, 072713 (2022).

[11] D. T. Michel, C. Sorce, R. Epstein, N. Whiting, I. V. Igumenshchev, R. Jungquist, and D. H. Froula, Shell trajectory measurements from direct-drive experiments, Rev. Sci. Instrum. **83**, 10E530 (2012).

[12] C. Stoeckl, R. Epstein, R. Betti, W. Bittle, J. A. Delettrez, C. J. Forrest, V. Yu. Glebov, V. N. Goncharov, D. R. Harding, I. V. Igumenshchev *et al.*, Monochromatic backlighting of direct-drive cryogenic DT implosions on OMEGA, Phys. Plasmas **24**, 056304 (2017).

[13] I. V. Igumenshchev, D. H. Edgell, V. N. Goncharov, J. A. Delettrez, A. V. Maximov, J. F. Myatt, W. Seka, A. Shvydky, S. Skupsky, and C. Stoeckl, Crossed-beam energy transfer in implosion experiments on OMEGA, Phys. Plasmas **17**, 122708 (2010).

[14] L. Spitzer, Jr. and R. Härm, Transport phenomena in a completely ionized gas, Phys. Rev. **89**, 977 (1953).

[15] S. Atzeni, A. Schiavi, F. Califano, F. Cattani, F. Cornolti, D. Del Sarto, T. V. Liseykina, A. Macchi, and F. Pegoraro, Fluid and kinetic simulation of inertial confinement fusion plasmas, Comput. Phys. Commun. **169**, 153 (2005).

[16] A. Colaïtis, I. Igumenshchev, J. Mathiaud, and V. Goncharov, Inverse ray tracing on icosahedral tetrahedron grids for non-linear laser plasma interaction coupled to 3D radiation hydrodynamics, J. Comput. Phys. **443**, 110537 (2021).

[17] A. Pineau, B. Chimier, S. X. Hu, and G. Duchateau, Modeling the electron collision frequency during solid-to-plasma transition of polystyrene ablator for direct-drive inertial confinement fusion applications, Phys. Plasmas **27**, 092703 (2020).

[18] L. J. Waxer, D. N. Maywar, J. H. Kelly, T. J. Kessler, B. E. Kruschwitz, S. J. Loucks, R. L. McCrory, D. D. Meyerhofer, S. F. B. Morse, C. Stoeckl *et al.*, High-energy petawatt capability for the OMEGA laser, Opt. Photonics News **16**, 30 (2005).

[19] C. Stoeckl, M. Bonino, C. Mileham, S. Regan, W. Theobald, T. Ebert, and S. Sander, Optimization of a short-pulse-driven Si He_α soft x-ray backlighter, High Energy Density Physics **41**, 100973 (2021).